Article

Not peer-reviewed version

Influence of Heat Treatment Temperature on the Electrochemical Properties of Cold-Rolled 0.2%C–3%Al–6/8.5%Mn–Fe Medium Manganese Steel

Jihui Luo *, Huixin Zuo , Zhichao Li , Huiping Li

Posted Date: 2 January 2025

doi: 10.20944/preprints202412.2617.v1

Keywords: medium manganese steel; heat treatment; polarization curve; impedance; corrosion

Article

Influence of Heat Treatment Temperature on the Electrochemical Properties of Cold-Rolled 0.2%C–3%Al–6/8.5%Mn–Fe Medium Manganese Steel

Jihui Luo [1,2,*], Huixin Zuo [2], Zhichao Li [2], Huiping Li [2]

[1] College of Materials Science and Engineering, Yangtze Normal University, Chongqing, P.R. China
[2] School of Materials Science and Engineering, Shandong University of Science and Technology, Qingdao, P.R. China
* Correspondence: 20170128@yzny.edu.cn(J.L.)

Abstract: The microstructure evolution, polarization curve and impedance of cold-rolled 0.2%C–3%Al–6/8.5%Mn–Fe steel under heat treatment temperatures of 600–800 ℃ holding 10 minutes were tested. The results show that the cold-rolled texture of the steel does not completely disappear at 600 ℃ and 650 ℃, exhibiting high charge transfer resistance R_c and corresponding corrosion potential E_{corr}. When the heat treatment temperature rises to 700 ℃, the texture begins to eliminate, the R_c begins to decrease, indicating a decrease in corrosion resistance. When the heat treatment temperature rises to 750 ℃ and 800 ℃, it can be found that the proportion of austenite begins to increase and the number of grain boundaries decrease, resulting in an increase in R_c and an improvement in the corrosion resistance of the steel. Compared to 6.5Mn steel, the higher Mn content in 8.5Mn steel results in better corrosion resistance after high-temperature heat treatment.

Keywords: medium manganese steel; heat treatment; polarization curve; impedance; corrosion

1. Introduction

The use of medium manganese steel in car body manufacturing leads to greater fuel efficiency due to its light weight and excellent mechanical properties. Its dual advantages in cost and performance make it the most promising advanced high-strength steel for the next generation of automobiles [1,2]. In recent years, a large number of scholars have studied the design of medium manganese steel alloy composition [3], control of rolling process [4] and optimization of heat treatment process [5], achieving a series of important results that have greatly promoted the development of medium manganese steel [6–8]. For instance, Li et al [9] studied the heat treatment of medium manganese steel. The results shows that the ultimate tensile strength of 1380 MPa and elongation of 39% was obtained after intercritical hardening at 630–650 °C and tempered at 200 °C.

On the other hand, corrosion performance has also become an important consideration in the industrial application of medium manganese steel [10–12]. Research has shown that steel is less prone to corrosion when subjected to small deformation, exhibiting strong corrosion resistance. However, as the deformation increases to a large extent, it can lead to a decrease in corrosion resistance [13,14]. Furthermore, studies suggest that the presence of Mn in medium manganese steel can affect the corrosion rate, which is influenced by other chemical elements [15].

However, there are still very few reports on the electrochemical properties of cold rolled medium manganese steel, especially the influence of subsequent heat treatment on the electrochemical properties of cold-rolled 0.2%C–3%Al–6/8.5%Mn–Fe. This work discusses the heat treatment of two cold-rolled medium manganese steels with different Mn contents: 0.2%C–3%Al–6%Mn–Fe (6Mn) and 0.2%C–3%Al–8.5%Mn–Fe (8.5Mn). The heat-treated samples were subjected to electrochemical experiments to explore the factors affecting the corrosion performance of medium manganese steel, providing theoretical guidance for the process design of medium manganese steel.

 doi:10.20944/preprints202412.2617.v1

2. Materials and Methods

The composition of experimental steels is given in Table 1. The steel ingots were heated at 1200 ℃ for 2 hours in a vacuum induction furnace, then hot forged into a bar with a cross-sectional size of 100 mm × 30 mm using Ø450×450 Two-high Reversing Hot Mill, followed by air cooling to room temperature. The bar was then soaked at 1200 ℃ for 2 hours and proceed with 7 passes of hot rolling into a 4 mm thick strip within the temperature range of 1150–850 ℃, and air cooled to room temperature.

Table 1. Chemical composition (wt.%) of the two steels.

Steel	C	Al	Mn	Fe
6Mn	0.20	3.20	6.0	90.60
8.5Mn	0.19	3.11	8.4	88.30

After holding the hot-rolled plate at 770–800 °C for 1 hour, quench it and then temper at 200 °C for 20 minutes. Use a 1:3 mixture of hydrochloric acid and water to acid wash the heat-treated steel plate, and then proceed to cold rolling using Four-high Cold Mill with Hydraulic Tension. After multiple rolling passes, reduce the thickness to 1mm.

Conducted heat treatment experiments on the samples, heating the temperature to 600 °C, 650 °C, 700 °C, 750 °C and 800 °C respectively, holding for 10 minutes, and then continuous annealing.

The microstructure was analyzed with the help of a field emission scanning electron microscope (SEM) (FEI NOVA NANOSEM 450). The electrochemical measurements were carried out at room temperature using an electrochemical work station (PARSTAT 2273) with Pt as the counter electrode, saturated calomel electrode as the reference electrode, and the heat-treated samples as the working electrode. For comparative purposes, the as-cold-rolled samples were also tested. A surface area of 1 cm^2 for each sample was exposed to an electrolyte solution of 3.5% NaCl. During the test, start by testing the open circuit potential curve with an experimental time set to 3600 s. The impedance spectra were obtained at the open circuit potentials. The frequency range was from 10,000 to 0.01 Hz with a sinusoidal excitation signal of 10 mV. Polarization curves were measured from -1.1 to -0.1 V at a constant rate of potential change of 10 $mV \cdot s^{-1}$. Subsequently, use EIS Spectrum Analyser software for fitting analysis of the electrochemical impedance spectra curve to obtain a simulated equivalent circuit diagram.

3. Results

3.1. Microstructure Evolution

0.2%C–3%Al–6/8.5%Mn–Fe is a type of light weight medium manganese steel with a dual-phase (ferrite and austenite). Figure 1 shows the microstructure of 6Mn steel after different heat treatment temperatures. It can be observed that after heat treatment at 600 °C and 650 °C, the 6Mn steel still retains a cold-rolled texture. As the heat treatment temperature increases to 700 °C and 750 °C, the dual-phase of the matrix gradually becomes clearer, with the light-colored protrusions being the austenite phase, appearing in fine stripes, and the dark-colored recesses being the ferrite. This is because the heat treatment temperature remains within the two-phase region of the iron-carbon phase diagram. When the temperature reaches 800 °C, the amount of austenite gradually increases, changing from a striped to a granular shape, and begins to grow gradually. This is because of austenite stability increased with increasing temperature [16].

 doi:10.20944/preprints202412.2617.v1

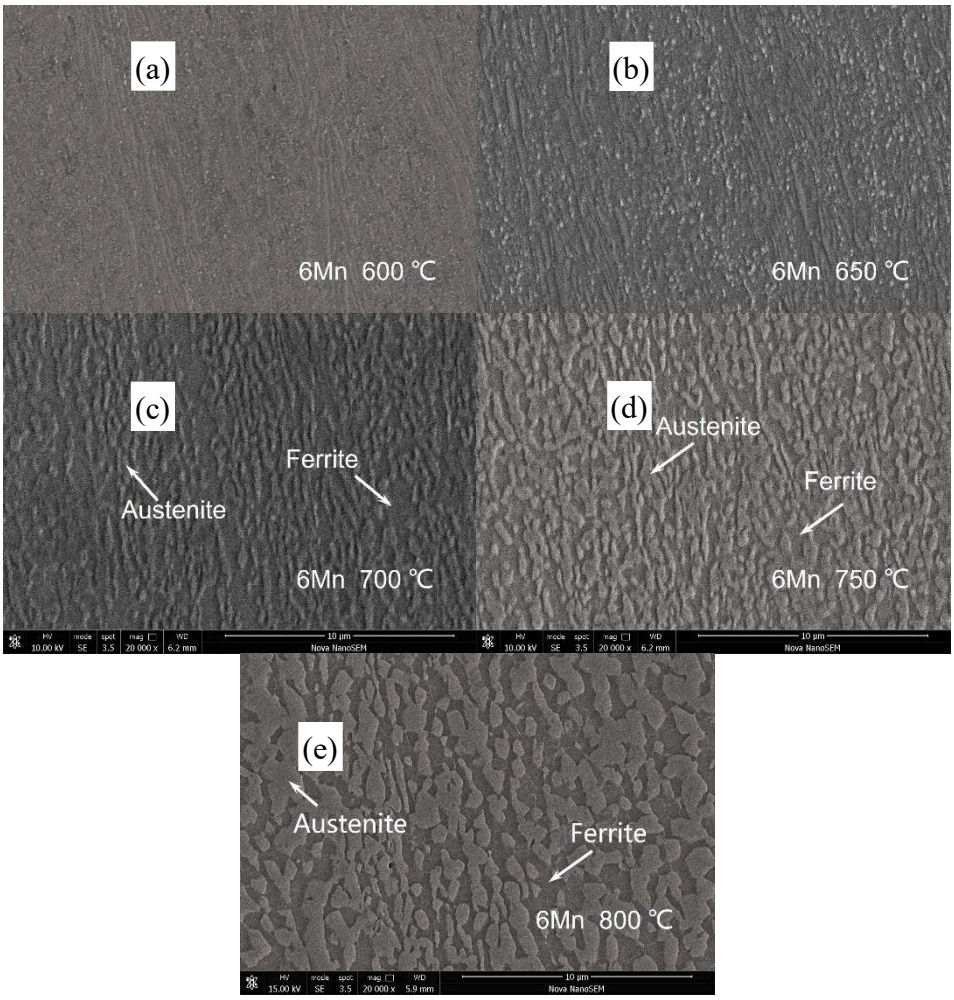

Figure 1. SEM of 0.2%C–3%Al–6%Mn–Fe steel with different heat treatment temperatures. (a) 600 ℃; (b) 650 ℃; (c) 700 ℃; (d) 750 ℃; (e) 800 ℃.

Figure 2 shows the microstructure of 8.5Mn steel after different heat treatments. It can be observed that 8.5Mn steel still retains the strip texture from cold rolling at a heat treatment temperature of 600 °C. As the heat treatment temperature increases to above 650 ℃, the texture begins to disappear. At 700 ℃, the dual-phase gradually appears in the matrix. While the temperature reaches 800 ℃, the amount of austenite starts to increase. A comparison between Figure 2 (e) and Figure 1 (e) reveals that after heat treatment at 800 ℃, the proportion of austenite in 8.5Mn steel is higher than that in 6Mn steel.

 doi:10.20944/preprints202412.2617.v1

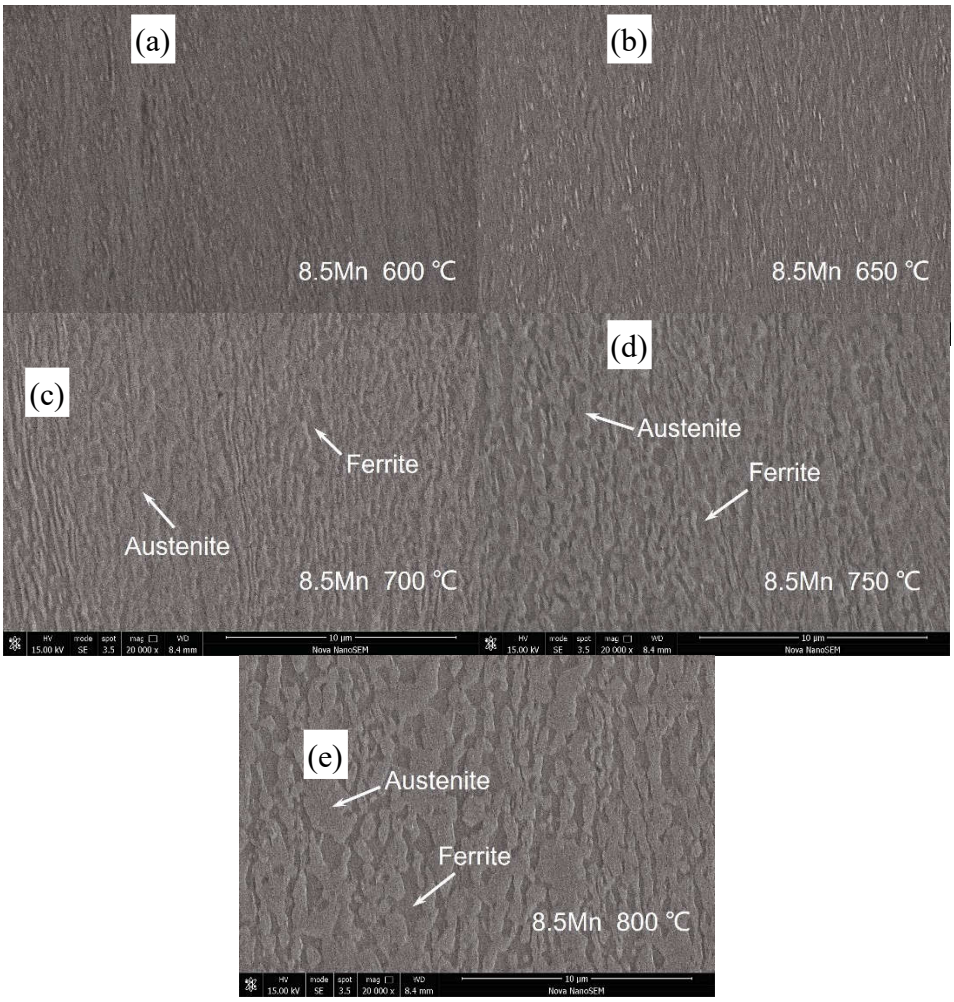

Figure 2. SEM of 0.2%C–3%Al–8.5%Mn–Fe steel with different heat treatment temperatures. (a) 600 ℃; (b) 650 ℃; (c) 700 ℃; (d) 750 ℃; (e) 800 ℃.

3.2. Electrochemical analysis

Polarization curve measurements were conducted on samples in cold-rolled and heat-treated, with the experimental results shown in Figure 3. Figure 3(a) shows the polarization curves of 6Mn steel at different heat treatment temperatures. Compared to the cold-rolled steel, the passivation zones of all anodic polarization curves after heat treatment have become shorter, indicating the absence of a passivation film on the metal surface. Figure 3(b) depicts the polarization curves of 8.5Mn steel at different heat treatment temperatures, also showing no obvious polarization zone. By extrapolating the polarization curves, the corrosion current density I_{corr}, the corresponding corrosion potential E_{corr}, and the pitting potential E_{pit} can be obtained, as shown in Tables 2 and 3.

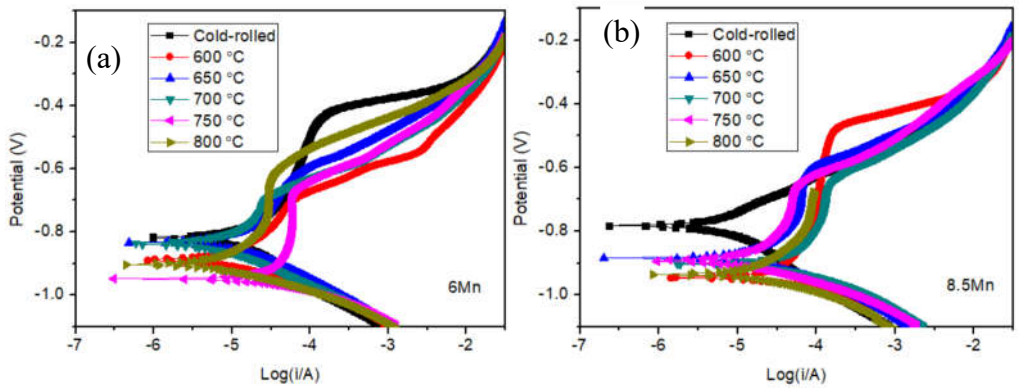

 doi:10.20944/preprints202412.2617.v1

Figure 3. Polarization curves of 0.2%C–3%Al–6/8.5%Mn–Fe steel with different heat treatment temperatures. (a) 6Mn; (b) 8.5 Mn.

Table 2. The polarization curves parameters of 6Mn steel derived from Figure 3(a).

Samples	E_{corr} (V)	I_{corr} (A/cm²)	E_{pit} (V)
Cold-rolled	-0.82	1.349×10-5	-0.44
600 ℃	-0.89	1.0×10-5	-0.70
650 ℃	-0.84	1.288×10-5	-0.65
700 ℃	-0.86	1.023×10-5	-0.70
750 ℃	-0.93	3.548×10-5	-0.68
800 ℃	-0.90	9.120×10-6	-0.64

Table 3. The polarization curves parameters of 8.5Mn steel derived from Figure 3(b).

Samples	E_{corr} (V)	I_{corr} (A/cm²)	E_{pit} (V)
Cold-rolled	-0.76	6.025×10-6	-
600 ℃	-0.92	7.943×10-5	-0.49
650 ℃	-0.88	1.995×10-5	-0.62
700 ℃	-0.90	4.786×10-5	-0.65
750 ℃	-0.89	1.445×10-5	-0.65
800 ℃	-0.92	2.238×10-5	-

The parameters from Tables 2 and 3 indicate that the heat treatment temperature has a certain influence on the E_{corr}, I_{corr}, and E_{pit}. In Table 1, the E_{corr} of the cold-rolled 6Mn steel is -0.82 V. After heat treatment, the E_{corr} of the steel begins to decrease. For example, it decreases to -0.89 V at 600 ℃ and to the lowest value of -0.93 V at 750 ℃. According to electrochemical theory, the more negative E_{corr}, the greater the material's corrosion tendency, and the more positive E_{corr}, the smaller the corrosion tendency. The above results indicate that the increase in heat treatment temperature weakens the corrosion resistance of the medium manganese steel. In Table 3, compared with the cold-rolled 8.5Mn steel, the E_{corr} of the 8.5Mn steel also shows a decreasing trend overall after heat treatment, but it is not significant.

In Table 2, the I_{corr} of cold-rolled 6Mn steel is 1.349×10^{-5} A/cm². After being subjected to a heat treatment at 600 ℃, I_{corr} begins to decrease to 1.0×10^{-5} A/cm². Subsequently, with an increase in the heat treatment temperature, I_{corr} starts to rise, but overall, it shows a gradual decrease. It reaches the lowest value of 9.120×10^{-6} A/cm² at 800 ℃. In Table 3, the I_{corr} of 8.5Mn steel also shows an overall decreasing trend, reaching the lowest value of 1.445×10^{-5} A/cm² at 750 ℃. Although the cold-rolled 6/8.5Mn steel has a smaller tendency for corrosion, its I_{corr} is the highest, resulting in a higher corrosion rate. After heat treatment, it is possible to reduce the corrosion rate, which is beneficial for improving the steel's corrosion resistance.

Furthermore, observing Table 2, it can be noted that with the increase in heat treatment temperature, the E_{pit} of 6Mn steel reaches its lowest value of -0.70 V at 600 ℃, and a relatively higher E_{pit} of -0.64 V at 800 ℃. Thermodynamically, this indicates a poorer tendency for pitting at this treatment temperature. On the other hand, the E_{pit} of 8.5Mn steel remains essentially unchanged, averaging around -0.6 V (Table 3). However, the E_{pit} of the as-cold-rolled 6Mn steel is higher, as the rolling deformation enhances the stability of 6Mn steel, making it less susceptible to corrosion.

The electrochemical impedance spectroscopy of 0.2%C–3%Al–6/8.5%Mn–Fe medium manganese steel is shown in Figure 4. It can be observed from the figure that the electrochemical

 doi:10.20944/preprints202412.2617.v1

impedance spectra at different heat treatment temperatures all exhibit capacitive arcs. The larger the radius of the capacitive arc, the greater the charge transfer resistance at the metal–solution interface, indicating better corrosion resistance of the metal. With the increase of the heat treatment temperature, the radius of the capacitive arc gradually decreases, reaching the minimum value at 700 °C. When the temperature rises above 750 °C, the radius of the capacitive arc begins to increase again. Therefore, the change trend of the capacitive arc radius indicates that the increase in heat treatment temperature first weakens and then strengthens its corrosion resistance. The corrosion resistance of 6Mn steel is optimal at 750 °C, while the corrosion resistance of 8.5Mn steel is optimal at 800 °C.

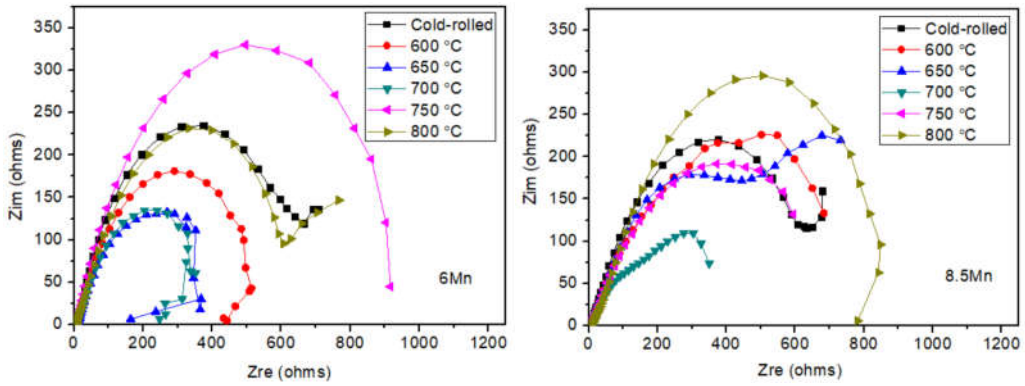

Figure 4. Nyquist diagrams of 0.2%C–3%Al–6/8.5%Mn–Fe steel with different heat treatment temperatures. (a) 6Mn; (b) 8.5 Mn.

Figure 5 shows the relationship between the modulus |Z| and frequency (Figures 5(a) and 5(c)), as well as the phase angle and frequency relationship (Figures 5(b) and 5(d)). It can be seen that at high frequencies, the modulus |Z| of 6/8.5Mn medium manganese steel is basically the same as that of the heat-treated. In the frequency range of 10-2 Hz to 10 Hz, there are significant fluctuations. The |Z| of 6Mn steel is larger when annealed at 750 °C, and in the Bode phase diagram, it has only one maximum phase angle (>50°), indicating relatively good corrosion resistance. Similarly, the |Z| of 8.5Mn steel is larger when heat-treated at 800 °C, and in the Bode phase diagram, its phase angle also has only one maximum value (>50°).

Preprints.org (www.preprints.org) | NOT PEER-REVIEWED | Posted: 2 January 2025 doi:10.20944/preprints202412.2617.v1

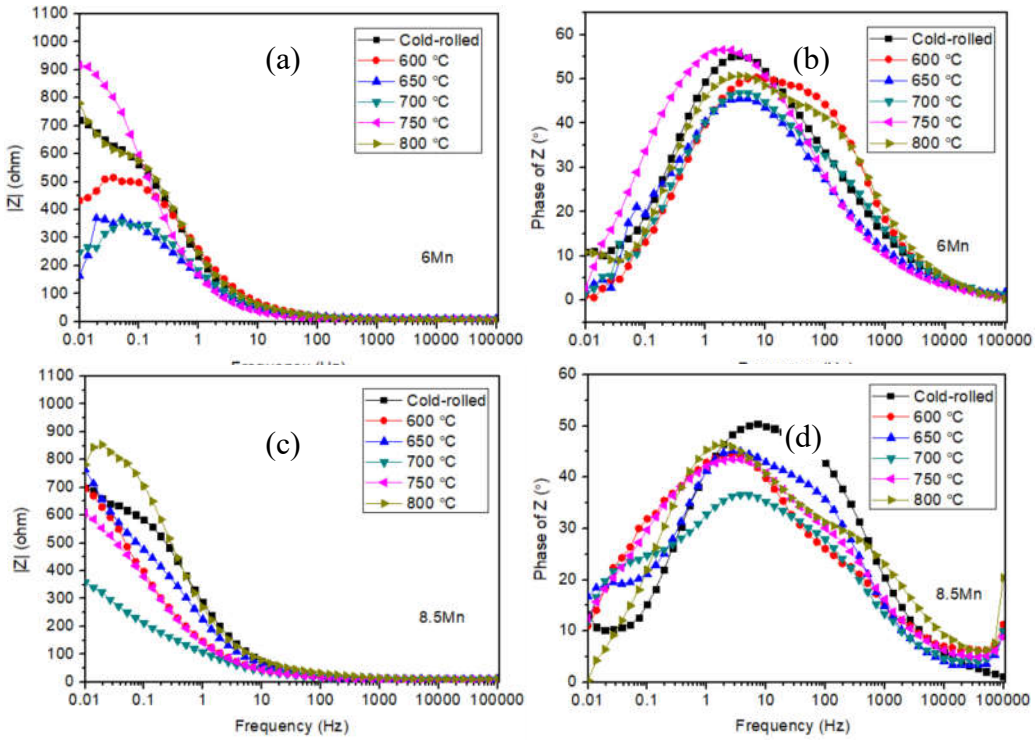

Figure 5. Bode curves of 0.2%C–3%Al–6/8.5%Mn–Fe steel with different heat treatment temperatures. (a) (b) 6Mn; (c) (d) 8.5 Mn.

By using the EIS Spectrum Analyser software, the Nyquist plots obtained for all samples in 3.5% NaCl solution were fitted and analysed. To ensure more accurate results of the fitting curve, it is essential to use an appropriate equivalent circuit [17]. Figure 6 shows the equivalent circuit diagram used for the fitting, and the fitting parameters for each component are presented in Table 4 (6Mn) and Table 5 (8.5Mn). The physical meanings of the components in the equivalent circuit diagram are as follows: R_s is the solution resistance, R_c is the charge transfer resistance, and the constant phase element (CPE) represents the double-layer capacitance at the electrode surface. P is the parameter for CPE, and n is the exponent of CPE, with a value range between 0.5 and 1. The magnitude of R_c can be used as a standard to measure the difficulty of electrochemical reactions in the corrosion system, making it a crucial parameter for evaluating the corrosion reaction rate of metals in this corrosion system.

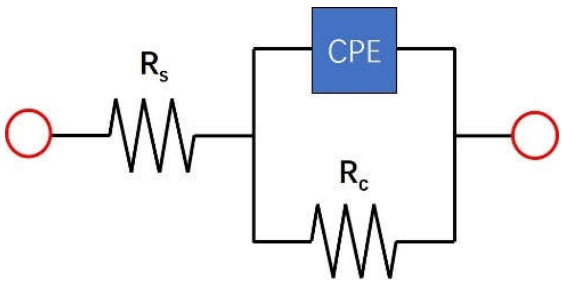

Figure 6. Equivalent circuit for the tested steel in 3.5% NaCl solution.

Table 4. Fitting parameters acquired from Nyquist diagrams of 6Mn in Figure 4(a).

Samples	$R_s(\Omega\cdot cm^2)$	CPE		$R_c(\Omega\cdot cm^2)$	% error
		$P(\Omega^{-1}\cdot s^{-n}\cdot cm^{-2})$	n		
Cold-rolled	7.6322	1.0864×10^{-3}	0.69098	760.51	≤4.6577
600 ℃	6.5467	7.5823×10^{-4}	0.69721	521.97	≤3.6619

 doi:10.20944/preprints202412.2617.v1

650 ℃	9.9172	1.5758×10^{-3}	0.63731	433.78	≤4.2213
700 ℃	8.0861	1.201×10^{-3}	0.65489	338.74	≤7.5118
750 ℃	7.5513	1.5256×10^{-3}	0.7112	1041.1	≤4.3011
800 ℃	6.1727	1.015×10^{-3}	0.65329	766.51	≤4.4369

Table 5. Fitting parameters acquired from Nyquist diagrams of 8.5Mn in Figure 4(b).

Samples	$R_s(\Omega\cdot cm^2)$	CPE		$R_c(\Omega\cdot cm^2)$	% error
		$P(\Omega^{-1}\cdot s^{-n}\cdot cm^{-2})$	n		
Cold-rolled	6.7926	8.1371×10^{-4}	0.66234	730.95	≤2.6804
600 ℃	8.8095	2.3881×10^{-3}	0.73174	974.33	≤7.9957
650 ℃	9.6177	1.3098×10^{-3}	0.59995	772.31	≤6.2676
700 ℃	7.9054	3.4156×10^{-3}	0.50568	436.55	≤5.5204
750 ℃	7.2716	2.3419×10^{-3}	0.55676	813.37	≤4.9458
800 ℃	9.8619	1.1333×10^{-3}	0.5655	1073.4	≤10.313

From Tables 4 and 5, it can be seen that the value of index n is between 0.6 and 0.8, indicating that the fitting results of the equivalent circuit are relatively accurate. Deviation from ideality indicates that this electrochemical process is a mixed behavior between ideal resistance and ideal capacitance. As the temperature of heat treatment increases, the value of R_c first decreases and then increases. The value of R_c is much larger than Rs, indicating that the corrosive solution itself has little influence on the electrochemical reaction in the corrosion system, and the corrosion rate is mainly determined by R_c. The R_c value of 6Mn steel is the highest at a heat treatment temperature of 750 ℃, reaching 1041.1 $\Omega\cdot cm^2$. The R_c value of 8.5Mn steel is the highest at a heat treatment temperature of 800 ℃, reaching 1073.4 $\Omega\cdot cm^2$. This indicates that at higher heat treatment temperatures, the corrosion resistance of the cold-rolled steel can be improved or restored.

4. Discussion

After cold rolling, steel will form a texture with a higher ability to resist corrosion and a higher E_{corr} [18–21]. After being heat-treated at 600 ℃, the texture begins to break down, causing the E_{corr} to decrease to -0.89 V (6Mn) and -0.92 V (8.5Mn). However, these traces of texture are not completely eliminated when annealed at lower temperatures (600 ℃ and 650 ℃), as seen clearly in Figures 1(a), 1(b) and Figures 2(a), 2(b) showing the microstructure in a streaked texture state. As the temperature further increases to 700 ℃, the texture disappears and its impact on corrosion begins to decrease, causing the E_{corr} to further decrease and the R_c to decrease as well.

When the influence of texture begins to weaken, the influence of grain size and phase becomes apparent. Due to the higher energy of grain boundaries compared to the matrix, grain boundaries can increase diffusion rates, reduce atomic coordination, enhance electron activity, lower surface work function, and increase R_c, making the surface more prone to electron loss or adsorption [22,23]. This can lead to corrosion at the grain boundaries. At heat treatment of 700 °C, the fine grains of medium manganese steel result in an excessive amount of grain boundaries, and the chemical reactivity of these boundaries starts to release. This leads to the lowest R_c at this temperature among all the samples (see Tables 4 and Table 5), causing the E_{corr} to decrease and the I_{corr} to increase, making corrosion easily occur. In Figure 5, both 6Mn steel and 8.5Mn steel exhibit the lowest impedance arc radius.

As the heat treatment temperature increases to 750 °C and 800 °C, the material undergoes recovery and recrystallization, causing the grain size to begin increasing and the number of grains to decrease. Previous research results also indicate that with the increase in heat treatment temperature, the grain size of medium manganese steel begins to increase [24,25], indicating a decrease in the

 doi:10.20944/preprints202412.2617.v1

quantity of grain boundaries. A reduced number of grain boundaries is beneficial for the corrosion resistance of the steel. Therefore, at 750 °C and 800 °C, the transfer resistance of 6Mn and 8.5Mn steel begins to increase, indicating an improvement in corrosion resistance.

As the temperature of heat treatment increases, the volume fraction of austenite also begins to increase (see Figure 1 and Figure 2). Research has shown that ferrite is more susceptible to corrosion, while austenite is less prone to corrosion [26,27]. This is also the reason for the continuous increase in the R_c of medium manganese steel under heat treatment conditions of 750 °C and 800 °C. Due to the increase in austenite content and fewer grains, deformation-induced medium manganese steel still exhibits good corrosion resistance even in the absence of a textured structure. An increased Mn content contributes to the stability of austenite [28,29]. Therefore, it can be observed that under the same heat treatment conditions, the R_c of 8.5Mn steel is significantly higher than that of 6Mn steel.

In summary, it can be seen that due to changes in the microstructure, several influencing factors (mainly phase, texture, and grain boundaries) interact and restrict each other, resulting in varying degrees of changes in the electrochemical performance. At low temperatures, texture plays a major role, while at high temperatures, grain boundaries and phase are important factors in improving the corrosion resistance of medium manganese steel.

5. Conclusions

This study investigated the electrochemical properties of cold-rolled 6Mn and 8.5Mn medium manganese steels after undergoing heat treatment at different temperatures. With the increasing of heat treatment temperature, the E_{corr} of both steels generally shows a decreasing trend. The trend of R_c initially decreases and then increases. At 700 ℃, the R_c of both 6Mn and 8.5Mn decrease to the minimum value, and then begin to increase again. At a heat treatment temperature of 750 ℃, the R_c of 6Mn steel reaches a maximum of 1041.1Ω·cm^2, while 8.5Mn steel reaches a maximum of 1073.4 Ω·cm^2 at 800 ℃.

Author Contributions: Conceptualization, J.L. and H.L.; methodology, H.Z.; software, J.L.; validation, J.L. and Z.L.; formal analysis, J.L.; investigation, J.L.; resources, J.L.; data curation, J.L. and H.Z.; writing—original draft preparation, J.L.; writing—review and editing, J.L.; visualization, J.L. and Z.L.; supervision, J.L. and Z.L.; project administration, J.L. and Z.L. All authors have read and agreed to the published version of the manuscript.

Data Availability Statement: The original contributions presented in this study are included in the article. Further inquiries can be directed to the corresponding author.

Acknowledgments: The authors are grateful for the guidance and experimental assistance provided by Associate Professor Lijie Yue and the master students Yibo Zhao and Yanping Wang from the School of Materials Science and Engineering at Shandong University of Science and Technology.

Conflicts of Interest: The authors declare no conflicts of interest.

References

1. Mohapatra, S.; Poojari, G.; Das, S.; Das, K. Insights into the dynamic impact behavior of intercritically annealed automotive-grade Fe–7Mn–4Al–0.18C steel. *Mat. Sci. Eng. A* **2023**, *887*, 145769.
2. Leták, R.; Jirková, H.; Kučerová, L.; Jeníček, Š.; Volák, J. Effect of forming and heat treatment parameters on the mechanical properties of medium manganese steel with 5% Mn. *Materials* **2023,** *16*, 4340.
3. Dykas, J.; Samek, L.; Grajcar, A.; Kozłowska A. Modelling of phase diagrams and continuous cooling transformation diagrams of medium manganese steels. *Symmetry* **2023,** *15*, 381.
4. Liu, T.; Dong, Y.; Qin, D.; Wu, H. Gao, X. Du, L. Effect of rolling temperature on microstructure and mechanical properties of medium manganese steel. *Mat Sci Eng A*. **2023,** *863*, 144547.
5. Mou, Y.; Li, Z.; Zhang, X.; Misra, D.; He, L.; Li, H. Design of an effective heat treatment involving intercritical hardening for high strength/high elongation of 0.2C–3Al–(6–8.5)Mn–Fe TRIP steels: microstructural evolution and deformation behavior. *Metals* **2019**, *9*, 1275.

 doi:10.20944/preprints202412.2617.v1

6. Hu, Z.; Fu, H. Effect of Si Content on Microstructure and Properties of Low-Carbon Medium-Manganese Steel after Intercritical Heat Treatment. *Metals* **2024,** *14(6)*, 675.
7. Li, Z.; Li, X.; Mou, Y.; Cai, Z.; Misra, D.; Zhang, X.; Li, H. The significance of microstructural evolution on governing impact toughness of Fe–0.2C–6Mn–3Al medium-Mn TRIP steel studied by a novel heat treatment. *Int. J. Mater. Res.* **2021,** *112(4)*, 271–279.
8. Qiao, Y.; Zheng, Z.; Yang, H.; Long, J.; Han, P. Recent progress in microstructural evolution, mechanical and corrosion properties of medium-Mn steel. *J. Iron. Steel. Res. Int.* **2023,** *30*, 1463–1476.
9. Li, Z.; Zhang, X.; Mou, Y.; Cai, Z.; Misra, D.; He, L.; Li, H.; Ding, H. Design of an effective heat treatment involving intercritical hardening for high-strength–high elongation of 0.2C–1.5Al–(6–8.5)Mn-Fe TRIP steels: microstructural evolution and deformation behaviour *Mater Sci Tech* **2020**, *36(4)*, 500–510.
10. Yan, X.; Kang, Shumei.; Xu M.; Li, P.; Corrosion Product Film of a Medium-Mn Steel Exposed to Simulated Marine Splash Zone Environment. *Materials* 2021, *14(19)*, 5652.
11. Mohapatra, S.; Palai, D.; Satpathy, B.; Das, S.; Das, K. Electrochemical study of intercritically annealed Fe–0.18C–7Mn–4Al steel. *Mater Today Commun.* **2023,** *34*, 105282.
12. Su, G.; Yu, C.; Zheng, H.; Gao, X.; Xie, H.; Huo, M.; Wu, H.; Xu, J.; Du, L.; Jiang, Z. The wet–dry cycling corrosion behavior of low-carbon medium manganese steel exposed to a 3.5% NaCl solution environment. *J. Mater. Eng. Perform.* **2022,** *31*, 7856–7869.
13. Choudhary, S.; Nanda, V.; Shekhar, S.; Garg, A.; Mondal, K. Effect of microstructural anisotropy on the electrochemical behavior of rolled mild steel. *J. Mater. Eng. Perform.* **2017,** *26(1)*, 185–194.
14. Wang, J.; Zhang, L. Effects of cold deformation on electrochemical corrosion behaviors of 304 stainless steel. *Anti-Corros Method M.* **2017**, *64(2)*, 252–262.
15. Su, G.; Gao, X.; Du, L.; Zhang, D.; Hu, J.; Liu, Z. Influence of Mn on the corrosion behaviour of medium manganese steels in a simulated seawater environment. *Int. J. Electrochem. Sci.* **2016,** *11*, 9447–9461.
16. Poling, W.A.; Moor, D.E.; Speer, J.G.; Findley, K.O. Temperature effects on tensile deformation behavior of a medium manganese TRIP Steel and a quenched and partitioned steel. *Metals* **2021**, *11*, 375.
17. Chen, J.; Zhu, Y.; Chen, X.; Ma, X.; Chen, B. Interfacial Microstructure and Cladding Corrosion Resistance of Stainless Steel/Carbon Steel Clad Plates at Different Rolling Reduction Ratios. *Metals* **2025,** *15*, 16.
18. Arafin, M.A.; Szpunar, J.A. A new understanding of intergranular stress corrosion cracking resistance of pipeline steel through grain boundary character and crystallographic texture studies. *Corros. Sci.* **2009,** *51*, 119–128.
19. Zhang, L.; Lin, N.; Zou, J.; et al. Super-hydrophobicity and corrosion resistance of laser surface textured AISI 304 stainless steel decorated with Hexadecyltrimethoxysilane (HDTMS). *Opt. Laser. Technol.* **2020**, *127*, 106146.
20. Shkatulyak, N.M.; Tkachuk, O.M. A role played by the crystallographic texture in the process of corrosion of hot-rolled rods made of carbon steel. *Mater. Sci.* **2012,** *48*, 153–161.
21. Wang, P.; Ma, L.; Cheng, X.; Li, X. Comparative effect of (111) and (110) crystallographic orientation on the passive behavior of low alloy steels in bicarbonate solution. *Appl. Surf. Sci.* **2021,** *561*, 150066.
22. Soleimani, M.; Mirzadeh, H.; Dehghanian, C. Effect of grain size on the corrosion resistance of low carbon steel. *Mater Res Express* **2020,** *7*, 016522.
23. Mishra, R.; Balasubramaniam, R. Effect of nanocrystalline grain size on the electrochemical and corrosion behavior of nickel. *Corros Sci.* **2004**, *46(12)*, 3019–3029.
24. Li, Q.; Sun, Y.; Zuo, H.; Feng, J.; Li, Z.; Cai, Z.; He, L.; Li, H. Microstructure evolution and mechanical properties of light medium manganese steel: different rolling directions during warm stamping. *J. Mater. Eng. Perform.* **2023**, 1–15.
25. Li, Z.; Ding, H.; Misra, R.D.K.; Cai, Z.; Li, H. Microstructural evolution and deformation behavior in the Fe–(6, 8.5)Mn–3Al–0.2C TRIP steels. *Mat. Sci. Eng. A* **2016,** *672*, 161–169.
26. Tsai, W.; Chen, J. Galvanic corrosion between the constituent phases in duplex stainless steel. *Corros Sci.* **2007,** *49(9)*, 3659–3668.
27. Wang, P.; Zheng, W.; Dai, X.; Zhang, P.; Wang, Y. Prominent role of reversed austenite on corrosion property of super 13Cr martensitic stainless steel. *J. Mater. Res. Technol.* **2023,** *22*, 1753–1767.

 doi:10.20944/preprints202412.2617.v1

28. Hu, B.; Zheng, Q.; Lu, Y.; Jia, C.; Liang, T.; Zheng, C. Stabilizing austenite via intercritical Mn partitioning in a medium Mn steel. *Scripta Mater.* **2023**, *225*, 115162.
29. Ding, R.; Zhang, C.; Wang, Y.; Liu, C.; Yao, Y.; Zhang, J.; Yang, Z.; Zhang, C.; Liu, Y.; Chen, H. Mechanistic role of Mn heterogeneity in austenite decomposition and stabilization in a commercial quenching and partitioning steel. *Acta Mater.* **2023**, *250*, 118869.